Ice injected into the tropopause by deep convection – Part 2: Over the Maritime Continent

Dion Iris-Amata[1], Dallet Cyrille[1], Ricaud Philippe[1], Carminati Fabien[2], Haynes Peter[3], and Dauhut Thibaut[4]

[1]CRNM, Meteo-France - CNRS, Toulouse, 31057, France
[2]Met Office, Exeter, Devon, EX1 3PB, UK
[3]DAMTP, University of Cambridge, Cambridge, CB3 0WA, UK
[4]Max Planck Institute for Meteorology, Hamburg, Germany

Correspondence: Iris-Amata Dion (iris.dion@meteo.fr)

Abstract. The amount of ice injected up to the tropical tropopause layer has a strong radiative impact on climate. In the tropics, the Maritime Continent (MariCont) region presents the largest injection of ice by deep convection into the upper troposphere (UT) and tropopause level (TL) (from results presented in the companion paper Part 1). This study focuses on the MariCont region and aims to assess the processes, the areas and the diurnal amount and duration of ice injected by deep convection over islands and over seas using a 2° × 2° horizontal resolution during the austral convective season of December, January and February. The model presented in the companion paper is used to estimate the amount of ice injected (ΔIWC) up to the TL by combining ice water content (IWC) measured twice a day in tropical UT and TL by the Microwave Limb Sounder (MLS; Version 4.2), from 2004 to 2017, and precipitation (Prec) measurement from the Tropical Rainfall Measurement Mission (TRMM; Version 007) at high temporal resolution (1 hour). The horizontal distribution of ΔIWC estimated from Prec (ΔIWC^{Prec}) is presented at 2° × 2° horizontal resolution over the MariCont. ΔIWC is also evaluated by using the number of lightning events (Flash) from the TRMM-LIS instrument (Lightning Imaging Sensor, from 2004 to 2015 at 1-h and 0.25°×0.25°resolutions). ΔIWC^{Prec} and ΔIWC estimated from Flash (ΔIWC^{Flash}) are compared to ΔIWC estimated from the ERA5 reanalyses (ΔIWC^{ERA5}) degrading the vertical resolution to that of MLS observations ($\left\langle \Delta IWC^{ERA5} \right\rangle$). Our study shows that, while the diurnal cycles of Prec and Flash are consistent to each other in timing and phase over lands and different over offshore and coastal areas of the MariCont, the observational ΔIWC range between ΔIWC^{Prec} and ΔIWC^{Flash} is small (they agree to within 4 – 22% over land and to within 7 – 53% over ocean) in the UT and TL. The reanalysis ΔIWC range between ΔIWC^{ERA5} and $\left\langle \Delta IWC^{ERA5} \right\rangle$ has been also found to be small in the UT (4 – 29 %) but large in the TL (55 – 78 %), highlighting the stronger impact of the vertical resolution on the TL than in the UT. Combining observational and reanalysis ΔIWC ranges, the total ΔIWC range is estimated in the UT between 4.2 and 10.0 mg m^{-3} (20 % of variability per study zone) over land and between 0.3 and 4.4 mg m^{-3} (30% of variability per study zone) over sea, and, in the TL, between 0.6 and 3.9 mg m^{-3} (70% of variability per study zone) over land and between 0.1 and 0.7 mg m^{-3} (80% of variability per study zone) over sea. Finally, from IWC^{ERA5}, Prec and Flash, this study highlights 1) ΔIWC over land has been found larger than ΔIWC over sea with a limit at 4.0 mg m^{-3} in the UT between minimum of ΔIWC estimated over land and maximum of

ΔIWC estimated over sea, and 2) small islands with high topography present the strongest amounts of ΔIWC such as the Java Island, the area of the largest ΔIWC in the UT (7.7 – 9.5 mg m^{-3} daily mean).

1 Introduction

In the tropics, water vapour (WV) and ice cirrus clouds near the cold point tropopause (CPT) have a strong radiative effect on climate (Stephens et al., 1991) and an indirect impact on stratospheric ozone (Stenke and Grewe, 2005). WV and water ice crystals are transported up to the tropopause layer by two main processes: a three-dimensional large-scale slow process (3-m month $^{-1}$), and a small scale fast convective process (diurnal timescale) (e.g. Fueglistaler et al., 2009; Randel and Jensen, 2013). Many studies have already shown the impact of convective processes on the hydration of the atmospheric layers from the upper troposphere (UT) to the lower stratosphere (LS) (e.g. Liu and Zipser, 2005; Jensen et al., , 2007; Dauhut et al., 2018; Dion et al., 2019). However, the amount of total water (WV and ice) transported by deep convection up to the tropical UT and LS is still not well understood. The vertical distribution of total water in those layers is constrained by thermal conditions of the CPT (Randel et al., 2006). During deep convective events, Dion et al. (2019) have shown that air masses transported up to 146 hPa in the UT and up to 100 hPa in the tropopause layer (TL) have ice to total water ratios of more than 50% and 70%, respectively, and that ice in the UT is strongly spatially correlated with the diurnal increases of deep convection, while WV is not. Dion et al. (2019) hence focused on the ice phase of total water to estimate the diurnal amount of ice injected into the UT and the TL over convective tropical areas, showing that it is larger over land than over ocean, with maxima over land of the Maritime Continent (MariCont), the region including Indonesian islands. For these reasons, the present study is focusing on the MariCont region in order to better understand small-scale processes impacting the diurnal injection of ice up to the TL.

A method to estimate the amount of ice injected into the UT and up to the TL over convective areas and during convective seasons has been proposed by Dion et al. (2019). This method provides an estimation of the amplitude of the diurnal cycle of ice in those layers using the twice daily Ice Water Content (IWC) measurements from the Microwave Limb Sounder (MLS) instrument and the full diurnal cycle of precipitation (Prec) measured by the Tropical Rainfall Measurement Mission (TRMM) instrument, at one hour resolution. The method first focuses on the increasing phase of the diurnal cycle of Prec (peak to peak from the diurnal Prec minimum to the diurnal Prec maximum) and shows that the increasing phase of Prec is consistent in time and in amplitude with the increasing phase of the diurnal cycle of deep convection, over tropical convective zones and during convective season. The amount of ice (ΔIWC) injected into the UT and the TL is estimated by relating IWC measured by MLS during the growing phase of the deep convection to the increasing phase of the diurnal cycle of Prec. Dion et al. (2019) conclude that deep convection over the MariCont region is the main process impacting the increasing phase of the diurnal cycle of ice in those layers.

The MariCont region is one of the main convective center in the tropics with the wettest troposphere and the coldest and driest tropopause (Ramage, 1968; Sherwood, 2000; Hatsushika and Yamazaki, 2001). Yang and Slingo (2001) have shown that over the Indonesian area, the phase of the convective activity diurnal cycle drifts from land to coastlines and to offshore areas. Even though authors have done a comprehensive work around the study of the diurnal cycle of precipitation and convection over the MariCont, the diurnal cycle of ice injected by deep convection up to the TL over this region is still not well understood. Millán et al. (2013) have tentatively evaluated the upper tropospheric diurnal cycle of ice from Superconducting Submillimeter-Wave Limb-Emission Sounder (SMILES) measurements over the period 2009-2010 but without differentiating land and sea over the MariCont, which caused their analysis to show little diurnal variation over that region. Dion et al. (2019) have 1) highlighted that the MariCont must be considered as two separate areas: the MariCont land (MariCont_L) and the MariCont ocean (MariCont_O), with two distinct diurnal cycles of the Prec and 2) estimated the amount of ice injected in the UT and the TL. Over these two domains, it has also been shown that convective processes are stronger over MariCont_L than over MariCont_O. Consequently, the amount of ice injected in the UT and the TL is greater over MariCont_L than over MariCont_O.

Building upon the results of Dion et al. (2019), the present study aims to improve the methodology of Dion et al. (2019) by i) studying smaller study zones than in Dion et al. (2019) and by distinguishing island and sea of the MariCont, ii) assessing the sensitivity of model to different proxies of deep convection and iii) assessing the amount of ice injected in the UT and the TL inferred by our model to that of ERA5 reanalyses. Based on space-borne observations and meteorological reanalyses, ΔIWC is assessed at a horizontal resolution of $2^\circ \times 2^\circ$ over 5 islands (Sumatra, Borneo, Java, Sulawesi and New Guinea) and 5 seas (West Sumatra Sea, Java Sea, China Sea, North Australia Sea, and Bismark Sea) of the MariCont during convective season (December, January and February, hereafter DJF) from 2004 to 2017. ΔIWC will be first estimated from Prec measured by TRMM-3B42. A sensitivity study of ΔIWC based on the number of flashes (Flash) detected by the TRMM Lightning Imaging Sensor (TRMM-LIS), an alternative proxy for deep convection as shown by Liu and Zipser (2008), is also proposed. Finally, we will use IWC calculated by the ERA5 reanalyses from 2005 to 2016 to estimate ΔIWC in the UT and the TL over each study zone and compare it to ΔIWC estimated from Prec and Flash.

The observational datasets used in our study are presented in Sect. 2. Method is recalled in Sect. 3. The amount of ice (ΔIWC) injected up to the TL estimated from Prec is evaluated in Sect. 4. Diurnal cycles of Prec and Flash are compared to each other over different areas of the MariCont in Sect. 5. Results of the estimated ΔIWC injected up to the UT and the TL over five islands and five seas of the MariCont are presented and compared with the ERA5 reanalyses in Sect. 6. Results are discussed in Sect. 7, and conclusions are drawn in Sect. 8. This paper contains many abbreviations and acronyms. To facilitate reading, they are compiled in the Acronyms list.

2 Datasets

This section presents the instruments and the reanalyses used for this study.

2.1 MLS Ice Water Content

The Microwave Limb Sounder (MLS, data processing algorithm version 4.2) instrument on board NASA's Earth Observing System (EOS) Aura platform (Waters et al., 2006; Livesey et al., 2018) launched in 2004 provides ice water content (IWC^{MLS}, mg m^{-3}) measurements. MLS provides IWC^{MLS} are given at 6 levels in the UTLS (82, 100, 121, 146, 177 and 215). However, we have chosen to study only two levels: an upper and a lower level of the TTL. Because the level at 82 hPa does not provide enough significant measurements of IWC to have a good signal-to-noise, we have selected 2 levels: 1) at 100 hPa as the upper level of the TTL (named TL for tropopause level), and 2) at 146 hPa as the lower level of the TTL (named UT for upper tropopshere). MLS follows a sun-synchronous near-polar orbit, completing 233 revolution cycles every 16 days, with daily global coverage every 14 orbits. The instrument is crossing twice a day the equator at fixed time, measuring IWC^{MLS} at 01:30 local time (LT) and 13:30 LT. The horizontal resolution of IWC^{MLS} measurements is $\sim$ 300 and 7 km along and across the track, respectively. The vertical resolution of IWC^{MLS} is 4 and 5 km at 146 and 100 hPa, respectively. Although optimal estimation is used to retrieve almost all other MLS products, a cloud-induced radiance technique is used to validate the MLS IWC (Wu et al., 2008; Wu et al., 2009). In our study, high horizontal resolution is now possible because we consider 13 years of MLS data, allowing to average the IWC^{MLS} measurements within the bins of horizontal resolution of 2° ×2° ($\sim$ 230 km). We select IWC^{MLS} during all austral convective seasons DJF between 2004 and 2017. The IWC measurements were filtered following the recommendations of the MLS team described in Livesey et al. (2018). The resolutions of IWC^{MLS} (horizontal along the path, horizontal perpendicular to the path, vertical) measured at 146 and 100 hPa are 300×7×4 km and 250×7×5 km, respectively. The precision of the measurement is 0.10 mg m^{-3} at 146 hPa and 0.25 to 0.35 mg m^{-3} at 100 hPa. The accuracy is 100% for values less than 10 mg m^{-3} at both levels and the valid range is 0.02-50.0 mg m^{-3} at 146 hPa and 0.1-50.0 mg m^{-3} at 100 hPa (Wu et al., 2008).

2.2 TRMM-3B42 Precipitation

The Tropical Rainfall Measurement Mission (TRMM) was launched in 1997 and provided measurements of Prec until 2015. TRMM is composed of five instruments, three of them are complementary sensor rainfall suite (PR, TMI, VIRS). TRMM had an almost circular orbit at 350 km altitude height performing a complete revolution in one and a half hour. The 3B42 algorithm product (TRMM-3B42) (version V7) has been created to estimate the precipitation and extend the precipitation product through 2019. TRMM-3B42 is a multi-satellite precipitation analysis composing a Global Precipitation Measurement (GPM) Mission. TRMM-3B42 is computed from the various precipitation-relevant satellite passive Microwave (PMW) sensors using GPROF2017 computed at the Precipitation Processing System (PPS) (e.g., GMI, DPR, Ku, Ka, Special Sensor Microwave Imager/Sounder [SSMIS], etc.) and including TRMM measurements from 1997 to 2015 (Huffman et al., 2007, 2010; and Huffman and Bolvin, 2018). Work is currently underway with NASA funding to develop more appropriate estimators for random error, and to introduce estimates of bias error (Huffman and Bolvin, 2018). Prec data are provided at a 0.25° × 0.25° ($\sim$ 29.2 km) horizontal resolution, extending from 50° S to 50° N (https://pmm.nasa.gov/data-access/downloads/trmm, last access: April 2019). Prec from TRMM-3B42 products depends on input from microwave and IR sensors (Huffman et al., 2007) and does

not differentiate between stratiform and convective precipitation. In our study, Prec from TRMM-3B42 is selected over the austral convective seasons (DJF) from 2004 to 2017 and averaged to a horizontal grid of 2° ×2° to be compared to IWC^{MLS}. The granule temporal coverage of TRMM-3B42 data is 3 hours, but the temporal resolution of individual measurements is 1 minute. Thus, it is statistically possible to degrade the resolution to 1 hour. TRMM-3B42 are provided in Universal Time that we converted into local time (LT). Details of the binning methodology of TRMM-3B42 is provided by Huffman and Bolvin (2018).

2.3 TRMM-LIS number of Flashes

The Lightning Imaging Sensor (LIS) aboard of the TRMM satellite measures several parameters relative to lightning. According to Christian et al. (2000), LIS used a Real-Time Event Processor (RTEP) that discriminates lightning event from Earth albedo light. A lightning event corresponds to the detection of a light anomaly on a pixel representing the most fundamental detection of the sensor. After a spatial and temporal processing, the sensor was able to characterize a flash from several detected events. The instrument detects lightning with storm-scale resolution of 3-6 km (3 km at nadir, 6 km at limb) over a large region (550-550 km) of the Earth's surface. LIS horizontal resolution is provided at 0.25°×0.10°. A significant amount of software filtering has gone into the production of science data to maximize the detection efficiency and confidence level. Thus, each datum is a lightning signal and not noise. Furthermore, the weak lightning signals that occur during the day are hard to detect because of background illumination. A real-tile event processor removes the background signal to enable the system and detect weak lightning and achieve a 90% detection efficiency during the day. LIS is thus able to provide the number of flashes (Flash) measured. The TRMM LIS detection efficiency ranges from 69% near noon to 88% at night. The LIS instrument performed measurements between 1 January 1998 and 8 April 2015. To be as consistent as possible to the MLS and TRMM-3B42 period of study, we are using LIS measurements during DJF from 2004 to 2015. The observation range of the sensor is between 38° N and 38° S. As LIS is on the TRMM platform, with an orbit that precesses, Flash from LIS can be averaged to obtain the full 24-h diurnal cycle of Flash over the study period with a 1-h temporal resolution. In our study, Flash measured by LIS is studied at 0.25° × 0.25° horizontal resolution to be compared to Prec from TRMM-3B42.

2.4 ERA5 Ice Water Content

The European Centre for Medium-range Weather Forecasts (ECMWF) Reanalysis 5, known as ERA5, replaces the ERA-Interim reanalyses as the fifth generation of the ECMWF reanalysis providing global climate and weather for the past decades (from 1979) (Hersbach, 2018). ERA5 provides hourly estimates for a large number of atmospheric, ocean and land surface quantities and covers the Earth on a 30 km grid with 137 levels from the surface up to a height of 80 km. Reanalyses such as ERA5 provide a physically constrained, continuous, global, and homogeneous representation of the atmosphere through a large number of observations (space-borne, air-borne, and ground-based) with short-range forecasts. Although there is no direct observation of atmospheric ice content in ERA5, the specific cloud ice water content (mass of condensate / mass of moist air) (IWC^{ERA5}) corresponds to the changes in the analysed temperature (and at low levels, humidity) which is mostly driven by the assimilation of temperature-sensitive radiances from satellite instruments (https://cds.climate.copernicus.eu/cdsapp!

/dataset/reanalysis-era5-pressure-levels-monthly-means?tab=form, last access: July 2019). IWC^{ERA5} used in our analysis is representative of non-precipitating ice. Precipitating ice, classified as snow water, is also provided by ERA5 but not used in this study in order to focus only on the injected and non-precipitating ice into the TTL. Furthermore, results from Duncan and Eriksson (2018) have highlighted that ERA5 is able to capture both seasonal and diurnal variability in cloud ice water but the reanalyses exhibit noisier and higher amplitude diurnal variability than borne out by the satellite estimates. The present study uses the IWC^{ERA5} at 100 and 150 hPa averaged over DJF from 2005 to 2016 with one-hour temporal resolution. IWC^{ERA5} is governed by the model microphysics which allows ice supersaturation with respect to ice (100-150% in relative humidity) but not with respect to liquid water. Although microwave radiances at 183 GHz (sensitive to atmospheric scattering induced by ice particles) (Geer et al., 2017) are assimilated, cloud and precipitations are used as control variable in the 4D-Var assimilation system and cannot be adjusted independently in the analysis (Geer et al., 2017). The microwave data have sensitivity to the frozen phase hydrometeors but mainly to larger particles, such as those in the cores of deep convection (Geer et al., 2017), but the sensitivity to cirrus clouds in ERA5 is strongly dependent on microphysical assumptions on the shape and size of the cirrus particles. Indirect feedbacks are also acting on cirrus representation in the model – e.g. changing the intensity of the convection will change the amount of outflow cirrus generated. This is why observations that affects the troposphere by changing for example the stability, the humidity, or the synoptic situation can affect the upper level ice cloud indirectly (Geer et al., 2017). IWC^{ERA5} is used to assess the amount of ice injected in the UT and the TL as estimated by the model developed in Dion et al. (2019) and in the present study. IWC^{ERA5} have been degraded along the vertical at 100 and 150 hPa ($\langle \Delta IWC^{ERA5} \rangle$) consistently with the MLS vertical resolution of IWC^{MLS} (5 and 4 km at 100 and 146 hPa, respectively) using an unitary box function (see section 7.2). IWC^{ERA5} and $\langle \Delta IWC^{ERA5} \rangle$ will be both considered in this study. IWC^{ERA5}, initially provided in kg kg^{-1}, has been converted into mg m^{-3} using the temperature provided by ERA5 in order to be compared with MLS IWC observations.

3 Methodology

This section summarizes the method developed by Dion et al. (2019) to estimate ΔIWC, the amount of ice injected into the UT and the TL. Dion et al. (2019) have presented a model relating Prec (as proxy of deep convection) from TRMM to IWC^{MLS} over tropical convective areas during austral convective season DJF. The IWC^{MLS} value measured by MLS during the growing phase of the convection (at x = 01:30 LT or 13:30 LT) is compared to the Prec value at the same time x in order to define the correlation coefficient (C) between Prec and IWC^{MLS}, as follows:

$$C = \frac{IWC_x^{MLS}}{Prec_x} \quad (1)$$

The diurnal cycle of IWC estimated ($IWC^{est}(t)$) can be calculated by using C applied to the diurnal cycle of Prec (Prec(t)), where t is the time, as follows:

$$IWC^{est}(t) = Prec(t) \times C \tag{2}$$

The amount of IWC injected up to the UT or the TL (ΔIWC^{Prec}) is defined by the difference between the maximum of IWC^{est} (IWC$^{est}_{max}$) and its minimum (IWC$^{est}_{min}$).

$$\Delta IWC^{Prec} = C \times (Prec_{max} - Prec_{min}) = IWC^{est}_{max} - IWC^{est}_{min} \tag{3}$$

where $Prec_{max}$ and $Prec_{min}$ are the diurnal maximum and minimum of Prec, respectively. Figure 1 illustrates the relationship between the diurnal cycle of Prec and the two MLS measurements at 01:30 LT and 13:30 LT. The growing phase of the convection is defined as the period of increase in precipitation from $Prec_{min}$ to $Prec_{max}$. The amplitude of the diurnal cycle is defined by the difference between $Prec_{max}$ and $Prec_{min}$. In Fig. 1, because the growing phase of the convection illustrated is happening during the afternoon, only the MLS measurement at 13:30 LT is used in the calculation of ΔIWC. IWC at 01:30 LT is not used in that case.

4 Horizontal distribution of ΔIWC estimated from Prec over the MariCont

4.1 Prec from TRMM related to IWC from MLS

In order to identify the main areas of injection of ice in the TL over the MariCont, Figure 2 presents different parameters associated to this area: a) the name of the main islands and seas over the MariCont, b) the elevation (http://www.soda-pro.com/web-services/altitude/srtm-in-a-tile, last access: June 2019), c) the daily mean of Prec at 0.25° × 0.25° horizontal resolution, d) the hour of the diurnal maxima of Prec at 0.25° × 0.25° horizontal resolution, and e) the daily mean ($I\bar{W}C = (IWC_{01:30} + IWC_{13:30}) \times 0.5$) of IWC^{MLS} at 146 hPa at 2° × 2° horizontal resolution. Several points need to be highlighted. Daily means of Prec over land and coastal parts are higher than over oceans (Fig. 2c). Areas where the daily mean of Prec is maximum are usually surrounding the highest elevation over land (e.g. over NewGuinea) and near coastal areas (North West of Borneo in the China Sea and South of Sumatra in the Java Sea) (Fig. 2b and c). The times of the maxima of Prec are over land during the evening (18:00-00:00 LT), over coast during the night-morning (00:00-06:00 TL) and over sea during the morning-noon and even evening depending of the sea considered (09:00-12:00 LT and 15:00-00:00 LT). These differences could illustrate the impact of the land/sea breeze within the 24 hours. The sea breeze during the day favours the land convection at the end of the day when land temperature surface is higher than oceanic temperature surface. During the night, the coastline sea surface temperature becomes larger than the land surface temperature and the land breeze favours systematically the convection development over coast. These observations are consistent with results presented in Qian (2008), explaining that high precipitation is mainly concentrated over land in the MariCont because of the strong sea-breeze convergence, but also because

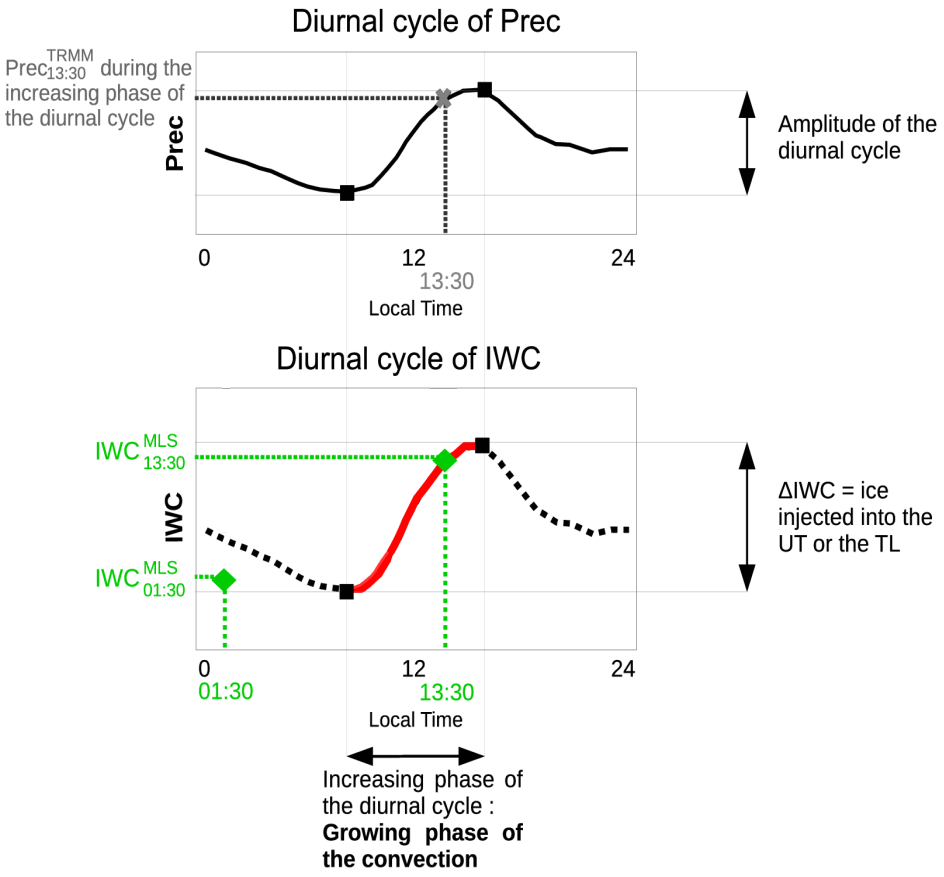

Figure 1. Illustration of the model used to estimate the amount of ice (ΔIWC) injected into the UT or the TL. Diurnal cycle of a proxy of deep convection (Prec) (a), diurnal cycle of ice water content (IWC) estimated from diurnal cycle of the proxy of deep convection (b). In red line, the increasing phase of the diurnal cycle. In black dashed line, the decreasing phase of the diurnal cycle. The green diamonds are the two IWC^{MLS} measurements from MLS. Grey thick cross represents the measurement of Prec during the growing phase of the convection ($\mathrm{Prec_x}$), used in the model. Maximum and minimum of the diurnal cycles are represented by black squares. Amplitude of the diurnal cycle is defined by the differences between the maximum and the minimum of the cycle.

of the combination with the mountain–valley winds and cumulus merging processes. Amplitudes of the diurnal cycles of Prec over the MariCont will be detailed as a function of island and sea in section 5. The location of the largest concentration of IWC (3.5 – 5.0 mg $\mathrm{m^{-3}}$, Fig. 2e) is consistent with that of Prec ($\sim$ 12 – 16 mm $\mathrm{day^{-1}}$) over the West Sumatra Sea, and over the South of Sumatra island. However, over North Australia seas (including the Timor Sea and the Arafura Sea), we observed large differences between Prec low values (4 – 8 mm $\mathrm{day^{-1}}$) and IWC large concentrations (4 – 7 mg $\mathrm{m^{-3}}$).

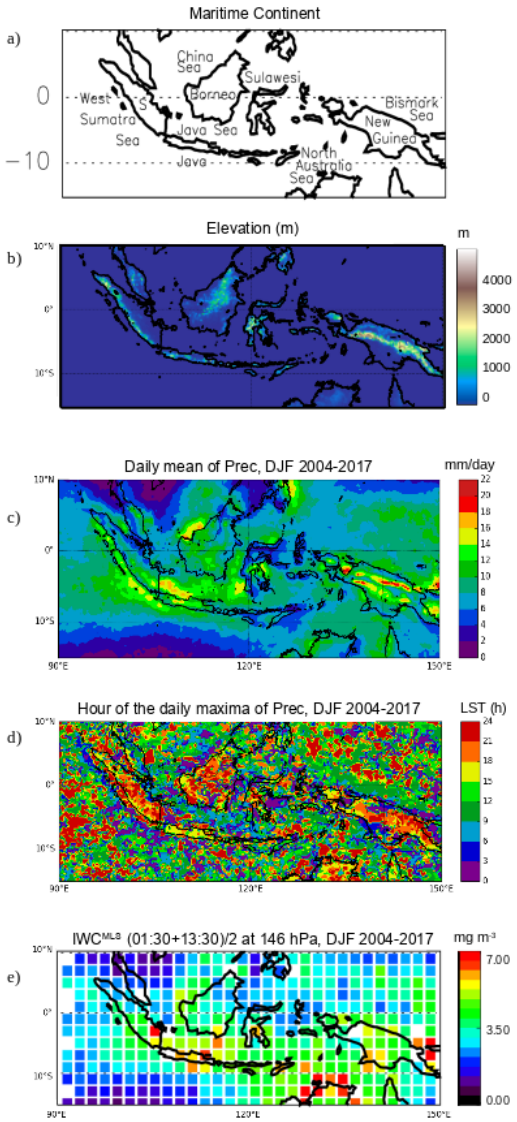

Figure 2. Main islands and seas of the MariCont (S is for Sumatra) (a), elevation from Solar Radiation Data (SoDa) (b); daily mean of Prec measured by TRMM over the Maritime Continent, averaged over the period of DJF 2004-2017 (c), hour (local solar time (LST)) of the diurnal maxima of Prec over the MariCont (d); daily mean (01:30 LT + 13:30 LT)/2 of IWC^{MLS} at 146 hPa from MLS over the MariCont averaged over the period of DJF 2004-2017 (e). Observations are presented with a horizontal resolution of $0.25^\circ \times 0.25^\circ$ (b,c and d) and $2^\circ \times 2^\circ$ (e).

4.2 Convective processes compared to IWC measurements

Although TRMM horizontal resolution is $0.25^\circ \times 0.25^\circ$, we require information at the same resolution as MLS IWC. From the diurnal cycle of TRMM Prec measurements, the duration of the increasing phase of Prec can be known for each $2^\circ \times 2^\circ$

pixel. The duration of the growing phase of the convection can then be defined from Prec over each pixel. Figures 3a and b present the anomaly (deviation from the mean) of Prec measured by TRMM–3B42 over the MariCont at 01:30 LT and 13:30 LT, respectively, only over pixels when the convection is in the growing phase. The anomaly of IWC measured by MLS over the MariCont is shown in Figs. 3c and d, over pixels when the convection is in the growing phase at 01:30 LT and 13:30 LT, respectively. Each pixel of Prec at 01:30 LT or 13:30 LT during the growing phase of the convection deviates by the average of the all Prec at 01:30 LT or 13:30 LT during the growing phase of the convection over the whole MariCont. The gray color denotes pixels for which convection is not ongoing. Some pixels can be presented on both sets of Prec and IWC panels in Figs. 3 when: 1) the onset of the convection is before 01:30 LT and the end is after 13:30 LT or 2) the onset of the convection is before 13:30 LT and the end is after 01:30 LT. Note that, whithin each 2°x2° pixel, at least 60 measurements of Prec or IWC at 13:30 LT or 01:30 LT over the period 2004-2017 have been selected for the average.

The Prec anomaly at 01:30 LT and 13:30 LT varies between -0.15 and +0.15 mm h^{-1}. The growing phase of the convection over land is mainly at 13:30 LT. At 13:30 LT, over land, the strongest Prec and IWC anomalies (+0.15 mm h^{-1} and +2.50 mg m^{-3}, respectively) are found over the Java island, and north of Australia for IWC. At 01:30 LT, the growing phase of the convection is found mainly over sea (while the pixels of the land are mostly gray), with maxima of Prec and IWC anomalies over coastlines and seas close to the coasts such as the Java Sea and the Bismark Sea. The IWC anomaly at 13:30 LT and 01:30 LT varies between -3 and +3 mg m^{-3}. Three types of areas can be distinguished from Fig. 3: i) area where Prec and IWC anomalies have the same sign (positive or negative either at 01:30 LT or 13:30 LT) (e.g. over Java, Borneo, Sumatra, Java Sea and coast of Borneo or the China Sea); ii) area where Prec anomaly is positive and IWC anomaly is negative (e.g. over West Sumatra Sea); and iii) area where Prec anomaly is negative and IWC anomaly is positive (e.g. over the North Australia Sea at 01:30 LT). Convective processes associated to these three types of areas over islands and seas of the MariCont are discussed in Sect. 6.

4.3 Horizontal distribution of ice injected into the UT and TL estimated from Prec

From the model developed in Dion et al. (2019) based on Prec from TRMM–3B42 and IWC from MLS and synthesized in section 2.4, we can calculate the amount of IWC injected (ΔIWC) at 146 hPa (UT, Figure 4a) and at 100 hPa (TL, Figure 4b) by deep convection over the MariCont. In the UT, the amount of IWC injected over land is larger (> 10 – 20 mg m^{-3}) than over seas (< 10 mg m^{-3}). South of Sumatra, Sulawesi, North of New Guinea and North of Australia present the largest amounts of ΔIWC over land (15 – 20 mg m^{-3}). Java Sea, China Sea and Bismark Sea present the largest amounts of ΔIWC over seas (7 – 15 mg m^{-3}). West Sumatra Sea and North Australia Sea present low values of ΔIWC (< 2 mg m^{-3}). We can note that the anomalies of Prec and IWC during the growing phase over North Australia Sea at 13:30 LT are positive (> 0.2 mg m^{-3}, Fig. 3a and b and > 2.5 mg m^{-3}, Fig. 3c and d, respectively). In the TL, the maxima (up to 3.0 mg m^{-3}) and minima (down to 0.2 – 0.3 mg m^{-3}) of ΔIWC are located within the same pixels as in the UT, although 3 to 6 times lower than in the UT. The decrease of ΔIWC with altitude is larger over land (by a factor 6) than over sea (by a factor 3). We can note that the similar pattern between the two layers come from the diurnal cycle of Prec in the calculation of ΔIWC at 146 and 100 hPa. Only the measured value of IWC^{MLS} at 146 and 100 hPa can explain the observed différences in ΔIWC values at these two

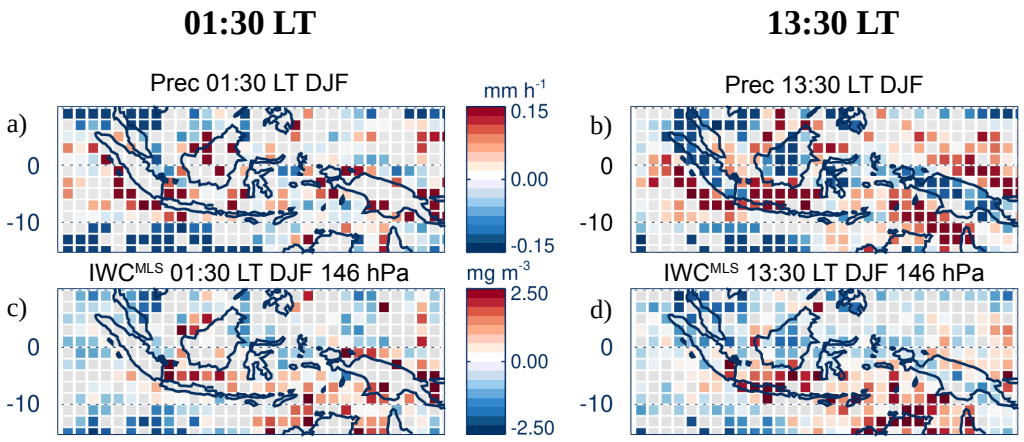

Figure 3. Anomaly (deviation from the mean) of Prec (a-b) and Ice Water Content (IWC^{MLS}) at 146 hPa (c-d), at 01:30 LT (left) and at 13:30 LT (right) over pixels where 01:30 LT and 13:30 LT are during the growing phase of the convection, respectively, averaged over the period of DJF 2004-2017. The gray color denotes pixels for which convection is not ongoing.

levels. Thus, similar ΔIWC patterns are expected between the two levels because, according to the model developed in Dion et al. (2019), the deep convection is the main process transporting ice into the UT and the TL during the growing phase of the convection. Convective processes associated to land and sea are further discussed in Sect. 6.

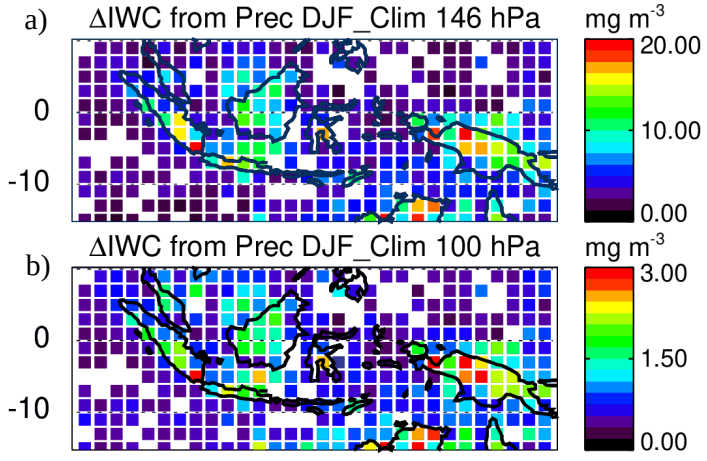

Figure 4. Daily amount of ice injected (ΔIWC) up to the UT (a) and up to the TL (b) estimated from Prec, averaged during DJF 2004-2017.

In order to better understand the impact of deep convection on the strongest ΔIWC injected per pixel up to the TTL, isolated pixels selected in Fig. 4a are presented separately in Figure 5a and f. This Figure shows the diurnal cycles of Prec in four pixels selected for their large ΔIWC in the UT ($\geq$ 15 mg m^{-3}, Fig. 5b, c, d, e), and the diurnal cycle of Prec in four pixels selected for their low ΔIWC in the UT (but large enough to observe the diurnal cycles of IWC between 2.0 and 5.0 mg m^{-3}, Fig. 5g, h, i, j). Pixels with low values of ΔIWC over land (Figs. 5g, h and i) present small amplitude of diurnal cycles of Prec ($\sim$ +0.5 mm h^{-1}), with maxima between 15:00 LT and 20:00 LT and minima around 11:00 LT. The pixel with low value of ΔIWC over sea (Fig. 5j) presents an almost null amplitude of the diurnal cycle of Prec with low value of Prec all day long ($\sim$ 0.25 mm h^{-1}). Pixels with large values of ΔIWC over land (Fig. 5b, c, d, e) present longer duration of the increasing phase of the diurnal cycle (from $\sim$ 09:00 LT to 20:00 – 00:00 LT) than the increasing phase of Prec diurnal cycle over pixels with low values of ΔIWC (from 10:00 LT to 15:00 – 19:00 LT). More precisely, pixels labeled 1 and 2 over New Guinea (Fig. 5d and e) and the pixel over South of Sumatra (Fig. 5c) show amplitude of diurnal cycle of Prec reaching 1.0 mm h^{-1}, while the pixel over North Australia (Fig. 5b) presents lower amplitude of diurnal cycle of Prec (0.5 mm h^{-1}).

IWC measured by MLS during the growing phase of deep convection and the diurnal cycle of IWC estimated from Prec are also shown on Fig. 5. For pixels with large values of ΔIWC, IWC observed by MLS is between 4.5 and 5.7 mg m^{-3} over North Australia Sea, South Sumatra and New Guinea. For pixels with low values of ΔIWC, IWC observed by MLS is found between 1.9 and 4.7 mg m^{-3}. To summarize, large values of ΔIWC are observed over land in combination to i) longer growing phase of deep convection (> 9 hours) and/or ii) large diurnal amplitude of Prec (> 0.5 mm h^{-1}).

In the next section, we estimate ΔIWC using another proxy of deep convection, namely Flash measurements from LIS.

5 Relationship between diurnal cycle of Prec and Flash over MariCont land and sea

Lightning is created into cumulonimbus clouds when the electric potential energy difference is large between the base and the top of the cloud. Lightning can appear at the advanced stage of the growing phase of the convection and during the mature phase of the convection. For these reasons, in this section, we use Flash measured from LIS during DJF 2004-2015 as another proxy of the deep convection in order to estimate ΔIWC (ΔIWC^{Flash}) and check the consistency with ΔIWC obtained with Prec (ΔIWC^{Prec}).

5.1 Flash distribution over the MariCont

Figure 6a presents the daily mean of Flash in DJF 2004-2015 at 0.25° × 0.25° horizontal resolution. Over land, Flash can reach a maximum of 10^{-1} flashes day^{-1} per pixel while, over seas, Flash are less frequent ($\sim 10^{-3}$ flashes day^{-1} day per pixel). When compared to the distribution of Prec (Fig. 2c), maxima of Flash are found over the same areas as maxima of Prec (Java, East of Sulawesi coast, Sumatra and North Australia lands). Over Borneo and NewGuinea, coastlines present more Flash ($\sim 10^{-2}$ flashes day^{-1}) than inland ($\sim 10^{-3}$ flashes day^{-1}). Differences between Flash and Prec distributions are found over North Australia Sea, with relatively large number of Flash ($\sim >10^{-2}$ flashes day^{-1}) compared to low Prec (4 – 10 mm day^{-1}) (Fig. 2c), and over NewGuinea where the number of Flash is relatively low ($\sim 10^{-2}$- 10^{-3} flashes day^{-1}) while Prec is high

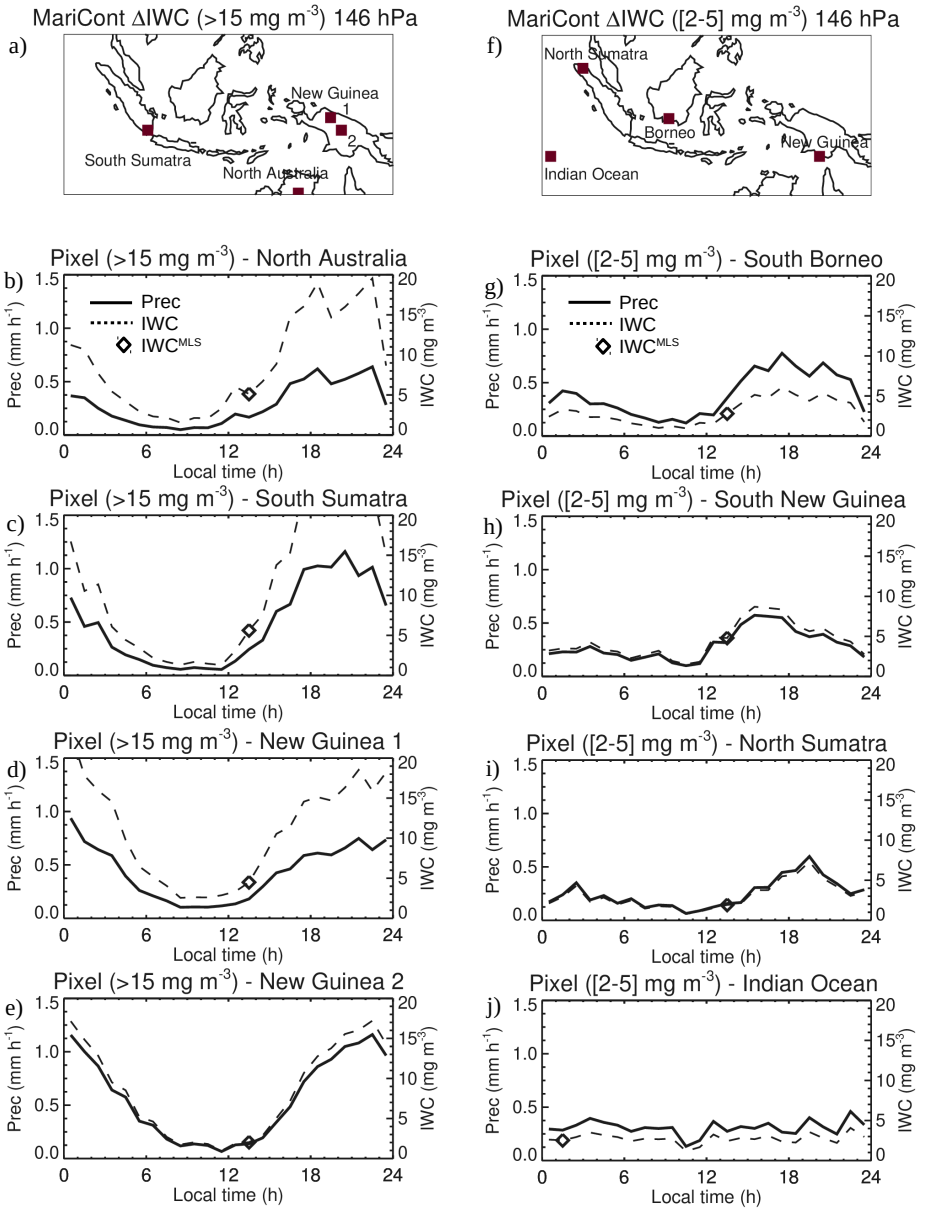

Figure 5. a) and f) location of $2^\circ \times 2^\circ$ pixels where ΔIWC have been found higher than 15 mg m^{-3} (in Fig. 4) and where ΔIWC have been found between 2 and 5 mg m^{-3} (in Fig. 4), respectively. Diurnal cycle of Prec (solid line): (b, c, d, e) over 4 pixels where ΔIWC have been found higher than 15 mg m^{-3} (in Fig. 4), (g, h, i, j) over 4 pixels where ΔIWC have been found between 2 and 5 mg m^{-3} (in Fig. 4), during DJF 2004-2017. The Diamond is IWC^{MLS} measured by MLS during the increasing phase of the convection. The dashed line is the diurnal cycle of IWC estimated from the diurnal cycle of Prec and from IWC^{MLS}.

($\sim$14 – 20 mm day^{-1}). Figure 6b shows the hour of the Flash maxima. Over land, the maximum of Flash is between 15:00 LT and 19:00 LT, slightly earlier than the maximum of Prec (Fig. 2d) observed between 16:00 LT and 24:00 LT. Coastal areas present similar hours of maximum of Prec and Flash, i.e between 00:00 LT and 04:00 LT although, over the West Sumatra Coast, diurnal maxima of both Prec and Flash happen 1–4 hours earlier (from 23:00-24:00 LT) than those of other coasts.

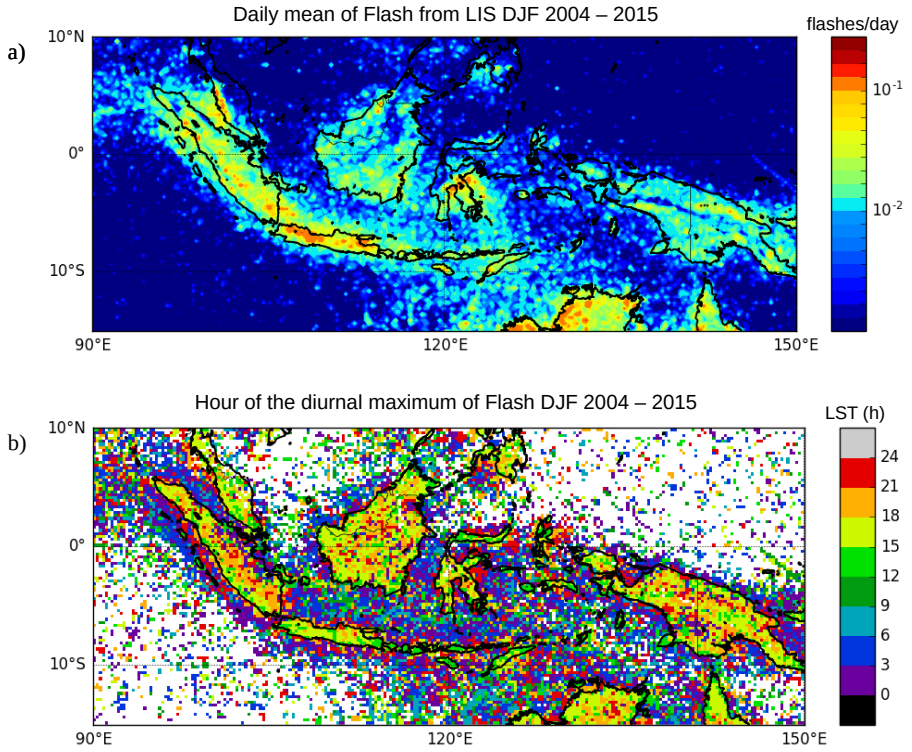

Figure 6. Daily mean of Flash measured by LIS averaged over the period DJF 2004-2015 (a); Hour (local solar time (LST)) of the diurnal maximum of Flash (b).

5.2 Prec and Flash diurnal cycles over the MariCont

This section compares the diurnal cycle of Flash with the diurnal cycle of Prec in order to assess the potential for Flash to be used as a proxy of deep convection over land and sea of the MariCont. Diurnal cycles of Prec and Flash over the MariCont land, coastline and offshore (MariCont_L, MariCont_C, MariCont_O, respectively) are shown in Figs. 7a–c, respectively. Within each 0.25° × 0.25° bin, land/coast/ocean filters were applied from the Solar Radiation Data (SoDa, http://www.soda-pro.com/web-services/altitude/srtm-in-a-tile). MariCont_C is the average of all coastlines defined as 5 pixels extending into the sea from the land limit. This choice of 5 pixels has been taken applying some sensitivity tests in order to have the best compromise between a high signal-to-noise ratio and a good representation of the coastal region. The MariCont_O is the average of all offshore pixels defined as sea pixels excluding 10 pixels (2000 km off the land) over the sea from the land coasts, thus coastline

pixels are excluded as well as all the coastal influences. MariCont_L is the area of all land pixels. A given $0.25° \times 0.25°$ pixel can contain information from different origins : land/coastlines or sea/coastlines. In that case, we can easily discriminate between land and coastlines or sea and coastlines by applying the land/ocean/coastlines filters. Consequently, this particular pixel will be flagged both as land and coastlines or sea and coastlines

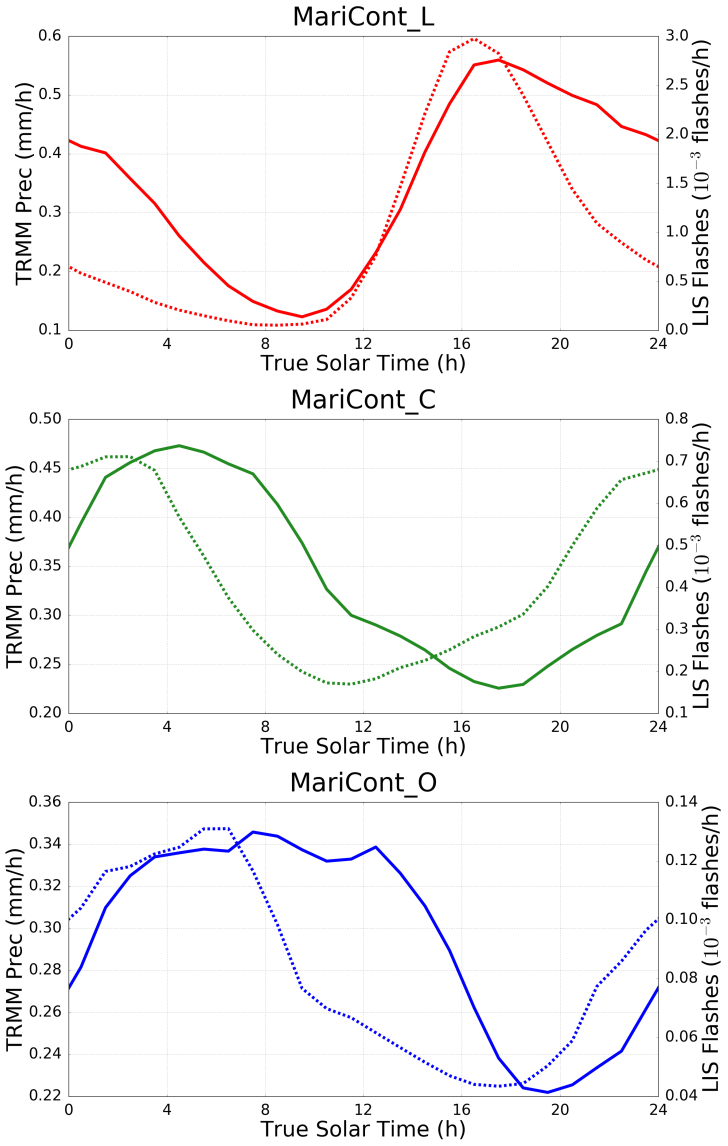

Figure 7. Diurnal cycle of Prec (solid line) and diurnal cycle of Flash (dashed line) over MariCont_L (top), MariCont_C (middle) and MariCont_O (bottom).

Over land, during the growing phase of the convection, Prec and Flash start to increase at the same time (10:00 LT – 12:00 LT) but Flash reaches a maximum earlier (15:00 LT – 16:00 LT) than Prec (17:00 LT – 18:00 LT). This is consistent with the

finding of Liu and Zipser (2008) over the whole tropics. Different maximum times could come from the fact that, while the deep convective activity intensity starts to decrease with the number of flashes, Prec is still high during the dissipating stage of the convection and takes longer times to decrease than Flash. Consequently, combining our results with the ones presented in Dion et al. (2019), Flash and Prec can be considered as good proxies of deep convection during the growing phase of the convection over the MariCont_L.

Over coastlines (Fig. 7c), the Prec diurnal cycle is delayed by about + 2 to 7 h with respect to the Flash diurnal cycle. Prec minimum is around 18:00 LT while Flash minimum is around 11:30 LT. Maxima of Prec and Flash are found around 04:00 LT and 02:00 LT, respectively. This means that the increasing phase of Flash is 2-3 h longer than that of Prec. These results are consistent with Mori et al. (2004) showing a diurnal maximum of precipitation in the early morning between 02:00 LT and 03:00 LT and a diurnal minimum of precipitation around 11:00 LT, over coastal zones of Sumatra. According to Petersen and Rutlegde (2001) and Mori et al. (2004), coastal zones are areas where precipitation results more from convective activity than from stratiform activity and the amplitude of diurnal maximum of Prec decreases with the distance from the coastline.

Over offshore areas (Fig. 7b), minima of diurnal cycle of Prec and diurnal cycle of Flash are in the late afternoon, between 16:00 LT and 17:00 LT (Flash) and 17:00 LT and 18:00 LT (Prec), whilst maxima of diurnal cycle of Prec and Flash are reached in the early morning, between 06:00 LT and 07:00 LT (Flash) and around 08:00 LT – 09:00 LT (Prec). Results over offshore areas are consistent with diurnal cycle of Flash and Prec calculated by Liu and Zipser (2008) over the whole tropical ocean, showing the increasing phase of the diurnal cycle of Flash starting 1–2 hours before the increasing phase of the diurnal cycle of Prec.

The time of transition from maximum to minimum of Prec is always longer than that of Flash. The period after the maximum of Prec is likely more representative of stratiform rainfall than deep convective rainfall. Consistently, model results from Love et al. (2011) have shown the suppression of the deep convection over offshore area in West of Sumatra from the early afternoon due to downwelling wavefront highlighted by deep warm anomalies around noon. According to the authors, later in the afternoon, gravity waves are forced by the stratiform heating profile and propagate slowly offshore. They also highlighted that the diurnal cycle of the offshore convection responds strongly to the gravity wave forcing at the horizontal scale of 4 km. To summarize, diurnal cycles of Prec and Flash show that:

i) over land, Flash increases proportionally with Prec during the growing phase of the convection,
ii) over coastlines, Flash increasing phase is advanced by more than 6–7 hours compared to Prec increasing phase,
iii) over offshore areas, Flash increasing phase is advanced by about 1–2 hours compared to Prec increasing phase.

In section 7, we investigate whether this time difference impacts the estimation of ΔIWC over land, coasts, and offshore areas.

5.3 Prec and Flash diurnal cycles and small-scale processes

In this subsection, we study the diurnal cycle of Prec and Flash at $0.25^\circ \times 0.25^\circ$ resolution over areas of deep convective activity over the MariCont. In line with the distribution of large value of Prec (Fig. 2), IWC (Fig. 3) and ΔIWC (Fig. 4), we have selected five islands and five seas over the MariCont. Diurnal cycles of Prec and Flash are presented over land for a) Java,

b) Borneo, c) New Guinea, d) Sulawesi and e) Sumatra as shown in Figure 8 and over sea for the a) Java Sea, b) North Australia Sea (NAusSea), c) Bismark Sea, d) West Sumatra Sea (WSumSea) and e) China Sea as shown in Figure 9. Diurnal cycles of IWC from ERA5 (IWC^{ERA5}) are also presented in Fig. 8 and 9 and will be discussed in Section 6.

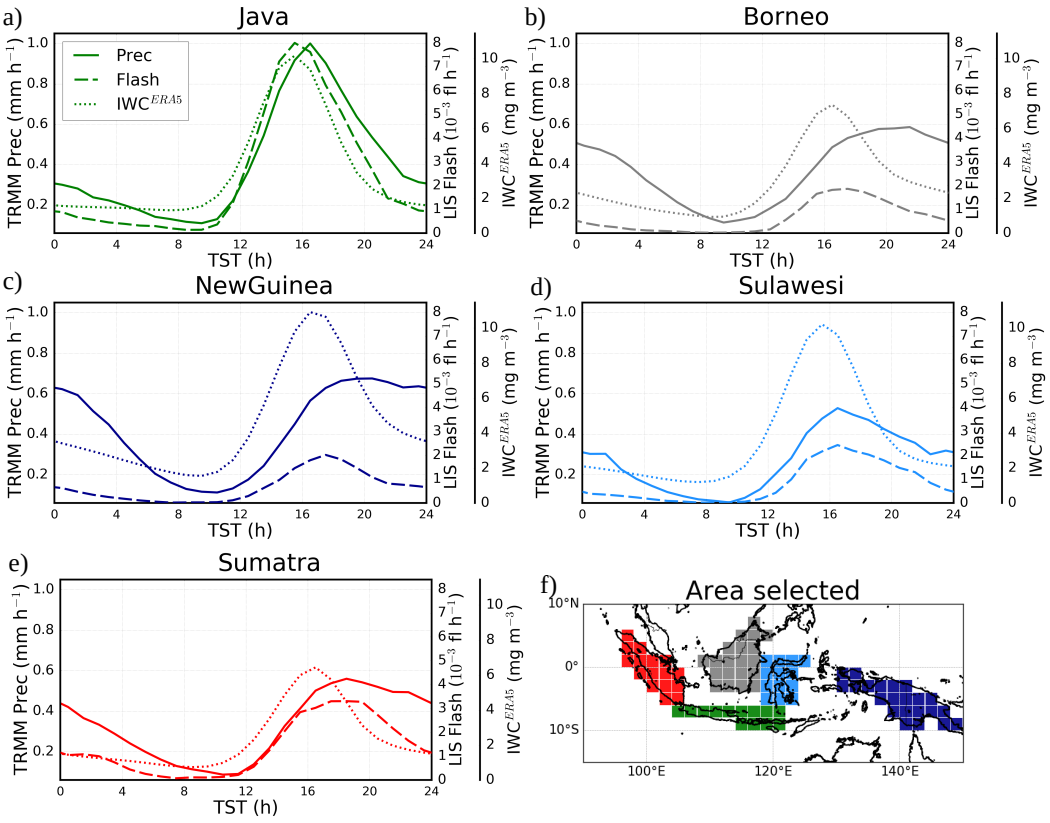

Figure 8. Diurnal cycles of Prec (solid line), Flash (dashed line) and IWC^{ERA5} from ERA5 at 150 hPa (dotted line) over MariCont islands: Java (a), Borneo (b), New Guinea (c), Sulawesi (d) and Sumatra (e) and map of the study zones over land (f).

Over land, the amplitude of the diurnal cycle of Prec is the largest over Java (Fig. 8a), consistent with Qian (2008), with a maximum reaching 1 mm h^{-1}, while, over the other areas, maxima are between 0.4 and 0.6 mm h^{-1}. Furthermore, over Java, the duration of the increasing phase in the diurnal cycle of Prec is 6-h consistent with that of Flash and elsewhere, the duration of the increasing phase is longer in Prec than in Flash by 1–2 h. The particularity of Java is related to the increasing phase of the diurnal cycle of Prec (6 h), that is faster than over all the other land areas considered in our study (7 – 8 h). The strong and rapid convective growing phase measured over Java might be explained by the fact that the island is narrow with high mountains (up to $\sim$ 2000 m of altitude, as shown in Fig. 2b) reaching the coast. The topography promotes the growth of intense and rapid convective activity. The convection starts around 09:00 LT, rapidly elevating warm air up to the top of the mountains. Around 15:00 LT, air masses cooled in altitude are transported to the sea favoring the dissipating stage of the convection. Sulawesi is

also a small island with high topography as Java. However, the amplitude of the diurnal cycle of Prec and Flash is not as strong as over Java. Other islands, such as Borneo, New Guinea and Sumatra, have high mountains but also large lowland areas. Mountains promote deep convection at the beginning of the afternoon while lowlands help maintain the convective activity through shallow convection and stratiform rainfall (Nesbitt and Zipser, 2003; Qian, 2008). Deep and shallow convection are then mixed during the slow dissipating phase of the convection (from $\sim$ 16:00 LT to 08:00 LT). However, because Flash are observed only in deep convective clouds, the decreasing phase of Flash diurnal cycles decreases more rapidly than the decreasing phase of Prec. The diurnal maxima of Prec found separately over the 5 islands of the MariCont are much higher than the diurnal maxima of Prec found over tropical land (South America, South Africa and MariCont_L) from Dion et al. (2019): $\sim$ 0.6 – 1.0 mm h^{-1} and $\sim$ 0.4 mm h^{-1}, respectively. However, the duration of the increasing phase of the diurnal cycle of Prec is consistent with the one calculated over tropical land by Dion et al. (2019).

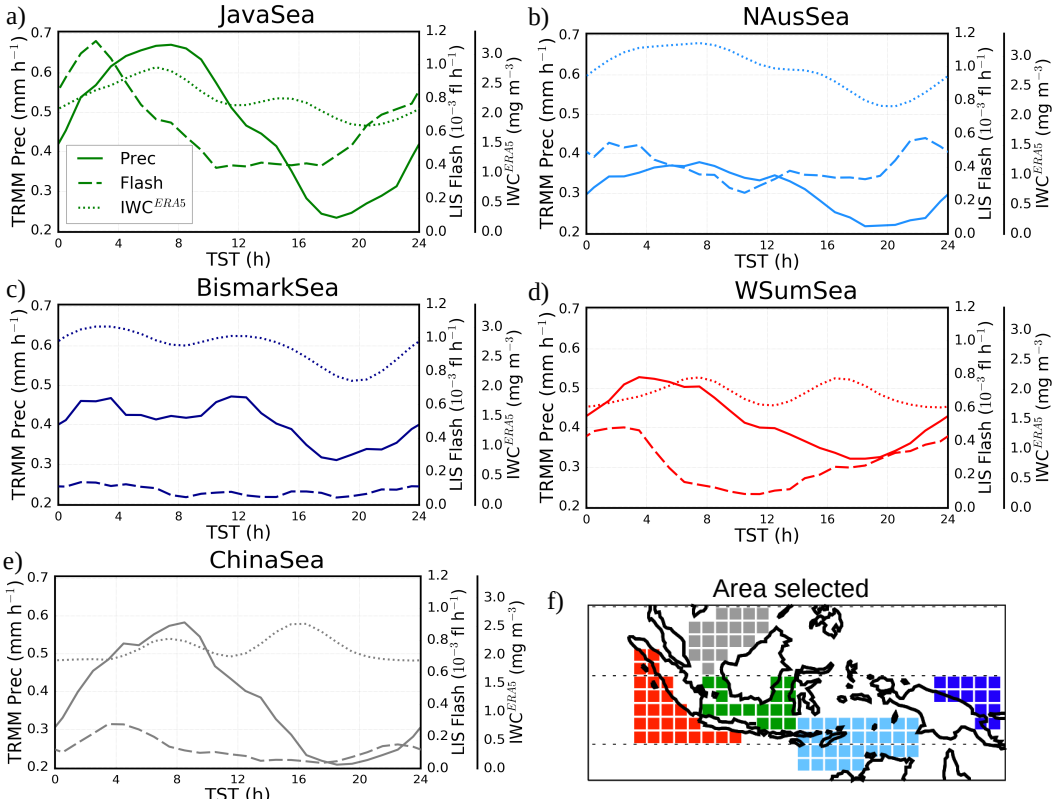

Figure 9. Diurnal cycles of Prec (solid line), Flash (dashed line) and IWC^{ERA5} from ERA5 at 150 hPa (dotted line) over MariCont seas: Java Sea (a), North Australia Sea (NAusSea) (b), Bismark Sea (c), West Sumatra Sea (WSumSea) (d), China Sea (e) and map of the study zones over sea (f).

Over sea, the five selected areas (Fig. 9a–e) show a diurnal cycle of Prec and Flash either coastline or offshore areas depending onthe area. The diurnal cycle of Prec and Flash over Java Sea is similar to the one over coastlines (Fig. 7c). Java Sea (Fig.

9a), an area mainly surrounded by coasts, shows the largest diurnal maximum of Prec ($\sim$ 0.7 mm h^{-1}) and Flash ($\sim$ 1.1 10^{-3} flashes h^{-1}) with the longest growing phase. In this area, land and sea breezes observed in coastal areas impact the diurnal cycle of the convection (Qian, 2008). During the night, land breeze develops from a temperature gradient between warm sea surface temperature and cold land surface temperature and conversely during the day. Over Java Sea, Prec is strongly impacted by land breezes from Borneo and Java islands (Qian, 2008), explaining why Prec and Flash reach largest values during the early morning. By contrast, NAusSea, Bismark Sea and WSumSea (Figs. 9b, c and d, respectively) present small amplitude of diurnal cycle. In our analysis, these three study zones are the areas including the most offshore pixels. Java Sea and WSumSea present a similar diurnal cycle of Prec and Flash, with Flash growing phase starting about 4 h earlier than that of Prec. China Sea also shows a diurnal maximum of Flash shifted by about 4 hours before the diurnal maximum of Prec, but the time of the diurnal minimum of Prec and Flash is similar. Over China Sea and Bismark Sea, the diurnal cycle of Flash shows a weak amplitude with maxima reaching only 0.1×0.2 10^{-3} flashes h^{-1}. Furthermore, over the Bismark Sea, while the diurnal minimum in Prec is around 18:00 LT, there are several local minima in Flash (08:00, 14:00 and 18:00 LT). Over NAusSea, the diurnal minimum of Prec is delayed by more than 7 hours compared to the diurnal minimum of Flash.

To summarize, over island, Flash and Prec convective increasing phases start at the same time and increase similarly but the diurnal maximum of Flash is reached 1–2 hours before the diurnal maximum of Prec. Over seas, the duration of the convective increasing phase and the amplitude of the diurnal cycles are not always similar depending on the area considered. The diurnal cycle of Flash is advanced by 4 hours over Java Sea and West Sumatra Sea and by more than 7 hours over North Australia Sea compared to the diurnal cycle of Prec. China Sea and Bismark Sea present the same time of the onset of the Flash and Prec increasing phase. In Section 7, we estimate ΔIWC over the 5 selected island and sea areas from Prec and Flash as a proxy of deep convection.

6 Horizontal distribution of IWC from ERA5 reanalyses

The ERA5 reanalyses provide hourly IWC at 150 and 100 hPa (IWC^{ERA5}). The diurnal cycle of IWC over the MariCont from ERA5 will be used to calculate ΔIWC from ERA5 in order to assess the horizontal distribution and the amount of ice injected in the UT and the TL deduced from our model combining MLS ice and TRMM Prec or MLS ice and LIS flash. Figures 10a, b, c and d present the daily mean and the hour of the diurnal maxima of IWC^{ERA5} at 150 and 100 hPa. In the UT, the daily mean of IWC^{ERA5} shows a horizontal distribution over the MariCont consistently with that of IWC^{MLS} (Fig. 2e), except over NewGuinea where IWC^{ERA5} (reaching 6.4 mg m^{-3}) is much stronger than IWC^{MLS} ($\sim$ 4.0 mg m^{-3}). The highest amount of IWC^{ERA5} is located over NewGuinea mountain chain and in the West coast of North Australia (reaching 6.4 mg m^{-3} in the UT and 1.0 mg m^{-3} in the TL). Over islands in the UT and the TL, the hour of the IWC^{ERA5} diurnal maximum is found between 12:00 LT and 15:00 LT over Sulawesi and New Guinea and between 15:00 LT and 21:00 LT over Sumatra, Borneo and Java, that is close to the hour of the diurnal maximum of Flash over islands (Fig. 6). Over sea, in the UT and the TL, the hour of the IWC^{ERA5} diurnal maximum is found between 06:00 LT and 09:00 LT over West Sumatra Sea, Java Sea, North

Australia Sea, between 06:00 LT and 12:00 LT over China Sea and between 00:00 LT and 03:00 LT over Bismark Sea. There are no significant differences between the hour of the maximum of IWC^{ERA5} in the UT and in the TL.

The diurnal cycles of IWC^{ERA5} at 150 hPa are presented in Figs. 8 and 9 over the selection of islands and seas of the MariCont together with the diurnal cycles of Prec and Flash. Over islands (Fig. 8), the maximum of the diurnal cycle of IWC^{ERA5} is found between 16:00 LT and 17:00 LT, consistent with the diurnal cycle of Prec and Flash. The duration of the increasing phase of the diurnal cycles of Prec, Flash and IWC^{ERA5} are all consistent to each other (6 – 8 h). Over sea (Fig. 9), the maximum of the diurnal cycle of IWC^{ERA5} is mainly found between 07:00 LT and 10:00 LT over Java Sea and North Australia Sea, consistently with the diurnal cycle of Prec and a second peak is found around 16:00 LT. Thus, the duration of the increasing phase of the diurnal cycles of IWC^{ERA5} is consistent with the one of Prec over these two sea study zones ($\sim$10 hours), but not with the one of Flash. Over Bismark Sea, the diurnal maxima of IWC^{ERA5} are found at 04:00 LT with a second peak later at noon. Over West Sumatra Sea, two diurnal maxima are found at 08:00 LT and 17:00 LT. Over China Sea, the diurnal maximum of IWC^{ERA5} are found at 16:00 LT with a second peak at 08:00 LT. These differences in the timing of the maximum of the diurnal cycle of Prec, Flash and IWCERA5 observed at small-scale over sea of the MariCont are not well understood. However, these differences do not impact on the calculation of the ΔIWCPrec, ΔIWCFlash or ΔIWCERA5. Results are presented Section 7.

7 Ice injected over a selection of island and sea areas

7.1 ΔIWC deduced from observations

Figure 11 synthesizes ΔIWC in the UT and the TL over the 5 islands and 5 seas of the MariCont studied in the previous section. Eqs. (1-3) are used to calculate ΔIWC from Prec (ΔIWC^{Prec}) and from Flash (ΔIWC^{Flash}). As presented in the previous section, Prec and Flash can be used as two proxies of deep convection, with differences more or less accentuated in their diurnal cycles as a function of the region considered. Thus, the observational ΔIWC range calculated between ΔIWC^{Prec} and ΔIWC^{Flash} provides an upper and lower bound of ΔIWC calculated from observational datasets.

In the UT (Fig. 11a), over islands, ΔIWC calculated over Sumatra, Borneo, Sulawesi and New Guinea varies from 4.9 to 6.9 mg m^{-3} whilst, over Java, ΔIWC reaches 7.9–8.7 mg m^{-3}. ΔIWC^{Flash} is generally greater than ΔIWC^{Prec} by less than 1.0 mg m^{-3} (((ΔIWC^{Flash}-ΔIWC^{Prec})/ΔIWC^{Flash})$\times$100 ranges from 4 to 22%) for all the islands, except for Java where is larger than ΔIWC^{Flash} by 0.7 mg m^{-3} (-8%). Over sea, ΔIWC varies from 1.2 to 4.4 mg m^{-3}. ΔIWC^{Flash} is greater than ΔIWC^{Prec} by 0.6 to 2.1 mg m^{-3} (31-50%), except for Java Sea, where ΔIWC^{Prec} is greater than ΔIWC^{Flash} by 0.2 mg m^{-3} (-7%). Over North Australia Sea, ΔIWC^{Flash} is almost twice as large as than ΔIWC^{Prec} (53%).

In the TL (Fig. 11b), the observational ΔIWC range is found between 0.7 and 1.3 mg m^{-3} over islands and between 0.2 and 0.7 mg m^{-3} over seas. The same conclusions apply to the observational ΔIWC range calculated between ΔIWC^{Prec} and ΔIWC^{Flash} in the TL as in the UT with differences less than 0.4 mg m^{-3}.

To summarize, independently of the proxies used for the calculation of ΔIWC, and at both altitudes, Java shows the largest injection of ice over the MariCont. Furthermore, it has been shown that both proxies can be used in our model, with more

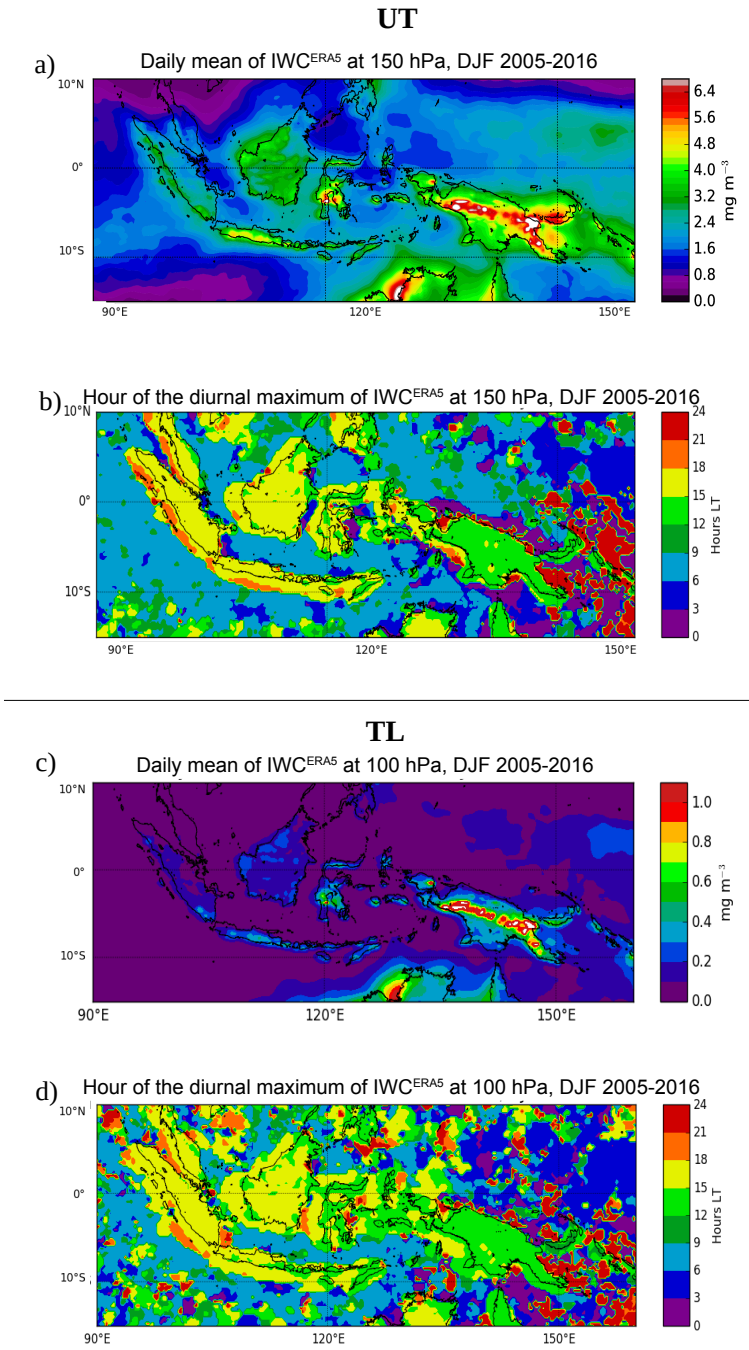

Figure 10. Daily mean of IWC^{ERA5} averaged over the period DJF 2005-2016 at 150 hPa (a) and at 100 hPa (c); Time (hour, local time (LT)) of the diurnal maximum of IWC^{ERA5} at 150 hPa (b) and at 100 hPa (d).

confidence over land: ΔIWC^{Prec} and ΔIWC^{Flash} are consistent to each other to within 4-22% over island and 7-53% over sea in the UT and the TL. The largest difference over sea is probably due to the larger contamination of stratiform precipitation included in Prec over sea.

7.2 ΔIWC deduced from reanalyses

ΔIWC from ERA5 (ΔIWC^{ERA5}) is calculated in the UT and the TL (z_0 = 150 and 100 hPa, respectively) as the max–min difference in the amplitude of the diurnal cycle. Consistently with the MLS observations, we have degraded the ERA5 vertical resolution to assess the impact of the vertical resolution on ΔIWC^{ERA5}. According to Wu et al. (2008), IWC^{MLS} estimation derived from MLS represent spatially-averaged quantities within a volume that can be approximated by a box of $300\times7\times4$ km^3 near the pointing tangent height. In order to compare IWC^{MLS} and IWC^{ERA5}, we degraded: 1) the horizontal resolution of ERA5 from $0.25°\times0.25°$ to $2°\times2°$ (200 km×200 km) and 2) ERA5 data by connecting the vertical profiles of IWC^{ERA5} with a unitary box function whose width is 5 and 4 km at 100 and 146 hPa, respectively.

Consistently with Livesey et al. (2018), we have fixed δz = 4 and 5 km at z_0 = 146 and 100 hPa, respectively. The ice injected from ERA5 at z_0 = 146 and 100 hPa with degraded vertical resolution ($\langle\Delta IWC_{z_0}^{ERA5}\rangle$) is thus calculated from $\langle IWC_{z_0}^{ERA5}\rangle$.

Figure 11 shows ΔIWC^{ERA5} and $\langle\Delta IWC_{z_0}^{ERA5}\rangle$ at z_0 = 150 and 100 hPa, over the island and the sea study zones. In the UT (Fig. 11a), over islands, ΔIWC_{150}^{ERA5} and $\langle\Delta IWC_{150}^{ERA5}\rangle$ calculated over Sumatra and Borneo vary from 4.9 to 7.0 mg m^{-3} (the relative variation calculated as $((\Delta IWC^{ERA5}\text{-}\langle\Delta IWC^{ERA5}\rangle)/\Delta IWC^{ERA5})\times100$ is 18-19 %) whilst ΔIWC_{150}^{ERA5} and $\langle\Delta IWC_{150}^{ERA5}\rangle$ over Java, Sulawesi and New Guinea reach 7.5–10.0 mg m^{-3} (∼19-22 % of variability per study zone). Over sea, ΔIWC_{150}^{ERA5} and $\langle\Delta IWC_{150}^{ERA5}\rangle$ vary from 0.35 to 1.1 mg m^{-3} (9 – 32 % of variability per study zone). Over island and sea, ΔIWC_{150}^{ERA5} is greater than $\langle\Delta IWC_{150}^{ERA5}\rangle$. The small differences between ΔIWC_{150}^{ERA5} and $\langle\Delta IWC_{150}^{ERA5}\rangle$ over island and sea in the UT support the fact that the vertical resolution at 150 hPa has a low impact on the estimated ΔIWC.

In the TL, over land, ΔIWC_{100}^{ERA5} and $\langle\Delta IWC_{100}^{ERA5}\rangle$ vary from 0.5 to 3.7 mg m^{-3} (∼68% of variability per study zone) with $\langle\Delta IWC_{100}^{ERA5}\rangle$ being larger than ΔIWC_{100}^{ERA5} by less than 2.1 mg m^{-3}. Over sea, ΔIWC_{100}^{ERA5} and $\langle\Delta IWC_{100}^{ERA5}\rangle$ vary from 0.05 to 0.4 mg m^{-3} (∼71 % of variability per study zone) with ΔIWC_{100}^{ERA5} lower than $\langle\Delta IWC_{100}^{ERA5}\rangle$ by less than 0.2 mg m^{-3}. The large differences between ΔIWC_{100}^{ERA5} and $\langle\Delta IWC_{100}^{ERA5}\rangle$ over island and sea in the TL support the fact that the vertical resolution at 100 hPa has a high impact on the estimation of ΔIWC.

7.3 Synthesis

The comparison between the observational ΔIWC range and the reanalysis ΔIWC range is presented in Fig. 11. In the UT, over land, observation and reanalysis ΔIWC ranges overlap (agree to within 0.1 to 1.0 mg m^{-3}), which highlights the robustness of our model over land, except over Sulawesi and New Guinea, where the observational ΔIWC range and the reanalysis ΔIWC range differ by 1.7 and 0.7 mg m^{-3}, respectively). Over sea, the observational ΔIWC range is systematically greater than the reanalysis ΔIWC range by ∼ 1.0 – 2.2 mg m^{-3} (75 %), showing a systematic positive bias and a too large variability range in our model over sea compared to ERA5. Combining observational and reanalysis ranges, the total ΔIWC variation range is

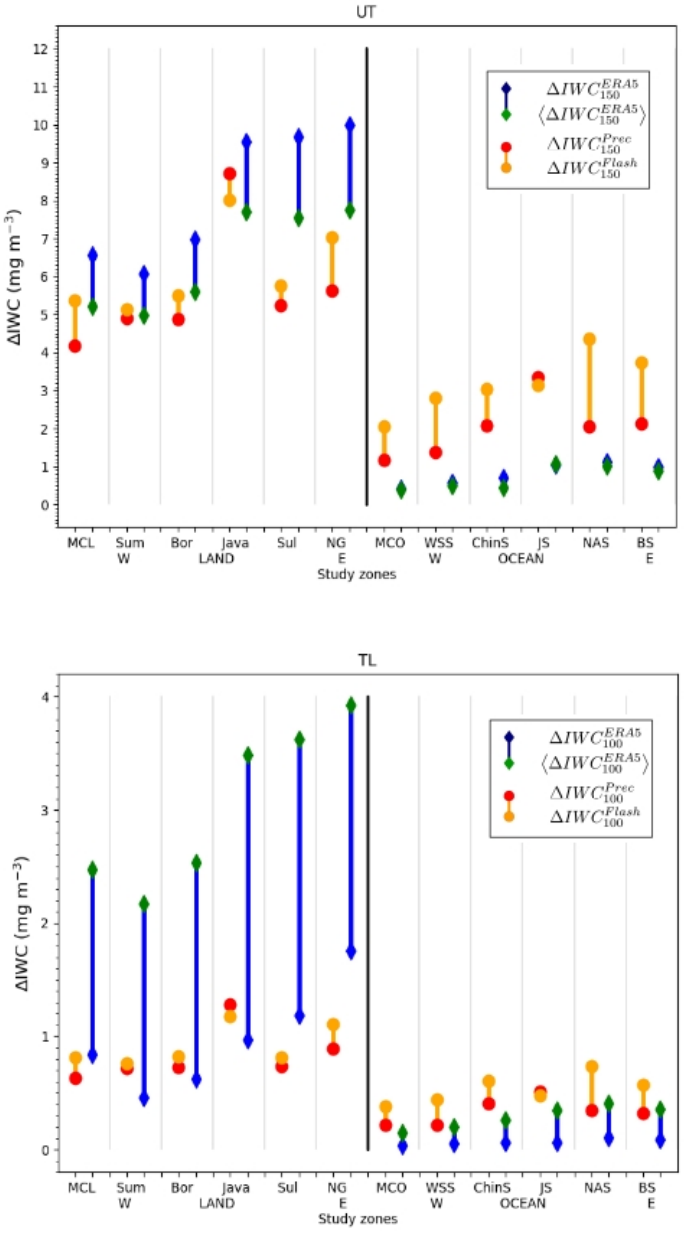

Figure 11. a) ΔIWC (mg m^{-3}) estimated from Prec (red) and Flash (orange) at 146 hPa and ΔIWC estimated from ERA5 at the level 150 hPa and at the level 150 hPa degraded in the vertical, over islands and seas of the MariCont: MariCont_L (MCL) and MariCont_O (MCO); from West (W) to East (E) over land, Sumatra (Sum), Borneo (Bor), Java, Sulawesi (Sul) and New Guinea (NG); and over seas, West Sumatra Sea (WSS), China Sea (ChinS), Java Sea (JS), North Australia Sea (NAS) and Bismark Sea (BS). b), Same as a) but for 100 hPa.

estimated in the UT between 4.2 and 10.0 mg m^{-3} ($\sim$ 20 % of variability per study zone) over land and between 0.3 and 4.4 mg m^{-3} ($\sim$ 30 % of variability per study zone) over sea and, in the TL, between 0.6 and 3.9 mg m^{-3} ($\sim$ 70 % of variability per study zone) over land, and between 0.1 and 0.7 mg m^{-3} ($\sim$ 80 % of variability per study zone) over sea.

The amounts of ice injected in the UT deduced from observations and reanalysis are consistent to each other over MariCont_L, Sumatra, Borneo and Java, with significant differences over Sulawesi, New Guinea (within 1.7 to 0.7 mg m^{-3}, respectively) and all individual offshore study zones (within 0.7 to 2.1 mg m^{-3}). The impact of the vertical resolution on the estimation of ΔIWC in the TL is certainly non negligible, with larger ΔIWC variability range in the TL (70 – 80 %) than in the UT (20 – 30 %). At both levels, observational and reanalyses ΔIWC estimated over land is more than twice as large as ΔIWC estimated over sea. Finally, whatever the level considered, although Java has shown particularly high values in the observational ΔIWC range compared to other study zones, the reanalysis ΔIWC range shows that Sulawesi and NewGuinea would also be able to reach similar high values of ΔIWC as Java.

8 Discussion on small-scale convective processes impacting ΔIWC over a selection of areas

Our results have shown that, in all the datasets used, Java island and Java Sea are the two areas with the largest amount of ice injected up to the UT and the TL over the MariCont land and sea, respectively. In this section, processes impacting ΔIWC in the different study zones are discussed.

8.1 Java island, Sulawesi and New Guinea

Sulawesi, New Guinea and particularly Java island have been shown as the areas of the largest ΔIWC in the UT and TL. Qian (2008) have used high resolution observations and regional climate model simulations to show the three main processes impacting the diurnal cycle of rainfall over the Java island. The main process explaining the rapid and strong peak of Prec during the afternoon over Java (Fig. 8a) is the sea-breeze convergence around midnight. This convergence caused by sea-breeze phenomenon increases the deep convective activity and impacts on the diurnal cycle of Prec and on the IWC injected up to the TL by amplifying their quantities. The second process is the mountain-valley wind converging toward the mountain peaks, and reinforcing the convergence and the precipitation. The land breeze becomes minor compared to the mountain-valley breeze and this process is amplified with the mountain altitude. As shown in Fig. 2b, NewGuinea has the highest mountain chain of the MariCont. The third process shown by Qian (2008) is precipitation that is amplified by the cumulus merging processes which is more important over small islands such as Java (or Sulawesi) than over large islands such as Borneo or Sumatra. Another process is the interaction between sea-breeze and precipitation-driven cold pools that generates lines of strong horizontal moisture convergence (Dauhut et al., 2016). Thus, IWC is increasing proportionally with Prec consistent with the results from Dion et al. (2019) and rapid convergence combined with deep convection transports elevated amounts of IWC at 13:30 LT (Fig. 3) producing high ΔIWC during the growing phase of the convection (Fig. 4 and Fig. 11) over Java.

8.2 West Sumatra Sea

In section 4.2, it has been shown that the West Sumatra Sea is an area with positive anomaly of Prec during the growing phase of the convection but negative anomaly of IWC, which differs from other places. These results suggest that Prec is representative not only of convective precipitation but also of stratiform precipitation. The diurnal cycle of stratiform and convective precipitations over West Sumatra Sea has been studied by Mori et al. (2004) using 3 years of TRMM precipitation radar (PR) datasets, following the 2A23Algorithm (Awaka, 1998). The authors have shown that rainfall over Sumatra is characterized by convective activity with a diurnal maximum between 15:00 and 22:00 LT while, over the West Sumatra Sea, the rainfall type is convective and stratiform, with a diurnal maximum during the early morning (as observed in Fig. 9). Furthermore, their analyses have shown a strong diurnal cycle of 200-hPa wind, humidity and stability, consistent with the PR over Sumatra West Sea and Sumatra Island. Stratiform and convective clouds are both at the origin of heavy rainfall in the tropics (Houze and Betts, 1981; Nesbitt and Zipser, 2003) and in the West Sumatra Sea, but stratiform clouds are mid-altitude clouds in the troposphere and do not transport ice up to the tropopause.Thus, over the West Sumatra Sea, the calculation of ΔIWC estimated from Prec is possibly overestimated because Prec include a non-negligible amount of stratiform precipitation over this area.

8.3 North Australia Sea and seas with nearby islands

The comparisons between Figs. 2c and 6a have shown strong daily mean of Flash ($10-2$ –$10-1$ flashes day-1) but low daily mean of Prec (2.0 – 8.0 mm day-1) over the North Australia Sea. Additionally, Fig. 11 shows that the strongest differences between ΔIWC^{Prec} and ΔIWC^{Flash} are found over the North Australia Sea, with ΔIWC^{Flash} greater than ΔIWC^{Prec} by 2.3 mg m-3 in the UT and by 0.4 mg m-2 in the TL (53% of variability between ΔIWC^{Flash} and ΔIWC^{Prec}). These results imply that the variability range in our model is too large and highlight the difficulty to estimate ΔIWC over this study zone. Furthermore, as for Java Sea or Bismarck Sea, North Australia Sea has the particularity to be surrounding by several islands. According to the study from Pope et al. (2008), the cloud size is the largest during the afternoon over the North Australia land, during the night over North Australia coastline and during the early morning over the North Australia sea. These results suggest that deep convective activity moves from the land to the sea during the night. Over the North Australia Sea, it seems that the deep convective clouds are mainly composed by storms with lightning but precipitationd are weak or do not reach the surface and evaporating before.

9 Conclusions

The present study has combined observations of ice water content (IWC) measured by the Microwave Limb Sounder (MLS), precipitation (Prec) from the algorithm 3B42 of the Tropical Rainfall Measurement Mission (TRMM), the number of flashes (Flash) from the Lightning Imaging Sensor (LIS) of TRMM with IWC provided by the ERA5 reanalyses in order to estimate the amount of ice injected (ΔIWC) in the upper troposphere (UT) and the tropopause level (TL) over the MariCont, from the method proposed in a companion paper (Dion et al., 2019). ΔIWC is firstly calculated using the IWC measured by MLS

(IWC^{MLS}) in DJF from 2004 to 2017 at the temporal resolution of 2 observations per day and Prec from TRMM-3B42 during the same period, to obtain a 1-hour resolution diurnal cycle. In the model used (Dion et al., 2019), Prec is considered as a proxy of deep convection impacting ice (ΔIWC^{Prec}) in the UT and the TL. While Dion et al. (2019) have calculated ΔIWC^{Prec} over large convective study zones in the tropics, we show the spatial distribution of ΔIWC^{Prec} into the UT and the TL at $2^\circ \times 2^\circ$ horizontal resolution over the MariCont, highlighting local areas of strong injection of ice up to 20 mg m^{-3} in the UT and up to 3 mg m^{-3} in the TL. ΔIWC injected in the UT and the TL has also been evaluated by using another proxy of deep convection: Flash measured by TRMM-LIS. Diurnal cycle of Flash has been compared to diurnal cycle of Prec, showing consistencies in 1) the spatial distribution of Flash and Prec over the MariCont (maxima of Prec and Flash located over land and coastline), and 2) their diurnal cycles over land (similar onset and duration of the diurnal cycle increasing phase). Differences have been mainly observed over sea and coastline areas, with the onset of the diurnal cycle increasing phase of Prec delayed by several hours depending on the considered area (from 2 to 7 h) compared to Flash. ΔIWC calculated by using Flash as a proxy of deep convection (ΔIWC^{Flash}) is compared to ΔIWC^{Prec} over five islands and five seas of the MariCont to establish an observational ΔIWC range over each study zone. ΔIWC is also estimated from IWC provided by the ERA5 reanalyses (ΔIWC^{ERA5} and IWC^{ERA5}, respectively) at 150 and 100 hPa over the study zones. We have also degraded the vertical resolution of IWC^{ERA5} to be consistent with that of IWC^{MLS} observations: 4 km at 146 hPa and 5 km at 100 hPa. The ΔIWC ranges calculated from observations and reanalyses were evaluated over the selected study zones (island and sea).

With the study of ΔIWC^{Prec}, results show that the largest amounts of ice injected in the UT and TL per $2^\circ \times 2^\circ$ pixels are related to i) an amplitude of Prec diurnal cycle larger than 0.5 mm h^{-1}, ii) values of IWC measured during the growing phase of the convection larger than 4.5 mg m^{-3} and iii) duration of the growing phase of the convection longer than 9 hours. The largest ΔIWC^{Prec} has been found over areas where the convective activity is the deepest. The observational ΔIWC range calculated between ΔIWC^{Prec} and ΔIWC^{Flash} has been found to be within 4 – 22 % over land and to within 7 – 53 % over sea. The largest differences between ΔIWC^{Prec} and ΔIWC^{Flash} over sea might be due to the combination of the presence of stratiform precipitation included into Prec and the very low values of Flash over seas (<10^{-2} flashes day^{-1}). The diurnal cycle of IWC^{ERA5} at 150 hPa is more consistent with that of Prec and Flash over land than over ocean. Finally, the observational ΔIWC range has been shown to be consistent with the reanalysis ΔIWC range to within 23 % over land and to within 30-50 % over sea in the UT and to within 49 % over land and to within 39 % over sea in the TL. Thus, thanks to the combination between the observational and reanalysis ΔIWC ranges, the total ΔIWC variation range has been found in the UT to be between 4.2 and 10.0 mg m^{-3} (to within 20 % per study zones) over land and between 0.3 and 4.4 mg m^{-3} (to within 30 % per study zones) over sea and, in the TL, between 0.6 and 3.9 mg m^{-3} (to within 70 % per study zones) over land and between 0.1 and 0.7 mg m^{-3} (to within 80% per study zones) over sea. The ΔIWC variation range in the TL is larger than that in the UT highlighting the stronger impact of the vertical resolution in the observations in the TL compared to the UT.

The study at small scale over islands and seas of the MariCont has shown that ΔIWC from ERA5, Prec and Flash in the UT agree to within 0 – 0.6 mg m^{-3} (8%) over MariCont_L, Sumatra, Borneo and Java with the largest values obtained over Java. However, while Java presents the largest amount of ΔIWC^{Prec} and ΔIWC^{Flash} in the UT and the TL (larger by about 1.0 mg m^{-3} in the UT and about 0.3 mg m^{-3} in the TL than other land study zones), New Guinea and Sulawesi reach similar ranges

of values of ice injected with ERA5 than

Java in the UT and even larger ranges of values as Java in the TL. Processes related to the strongest amount of ΔIWC injected into the UT and the TL have been identified as the combination of sea-breeze, mountain-valley breeze and merged cumulus, such as over NewGuinea and accentuated over small islands with high topography such as Java or Sulawesi.

Author contributions. IAD analysed the data, formulated the model and the method combining MLS, TRMM and LIS data and took primary responsibility for writing the paper. CD has treated the LIS data, provided the Figures with Flash datasets, gave advices on data processing and contributed to the Prec and Flash comparative analysis. PR strongly contributed to the design of the study, the interpretation of the results and the writing of the paper. PR, FC, PH and TD provided comments on the paper and contributed to its writing.

Acknowledgements. We thank the National Center for Scientific Research (CNRS) and the Excellence Initiative (Idex) of Toulouse, France to fund this study and the project called Turbulence Effects on Active Species in Atmosphere (TEASAO – http://www.legos.obs-mip.fr/projets/axes-transverses-processus/teasao, Peter Haynes Chair of Attractivy). We would like to thank the teams that have provided the MLS data (https://disc.gsfc.nasa.gov/datasets/ML2IWC_V004, last access: June 2019), the TRMM data (https://pmm.nasa.gov/data-access/downloads/trmm), the LIS data (https://ghrc.nsstc.nasa.gov/lightning/data/data_lis_trmm.html, last access: June 2019), the ERA5 Reanalysis data (https://cds.climate.copernicus.eu/cdsapp/dataset/reanalysis\protect\discretionary{\char\hyphenchar\font}{}{}era5, last access: June 2019), and the NCEP Reanalysis data provided by the NOAA/OAR/ESRL PSD, Boulder, Colorado, USA, (https://www.esrl.noaa.gov/psd/, last access: June 2019).

References

J. Awaka. Algorithm 2A23—Rain type classification. In Proc. Symp. on the Precipitation Observation from Non-Sun Synchronous Orbit, pages 215–220, 1998.

R. E. Carbone, J. W. Wilson, T. D. Keenan, and J. M. Hacker. Tropical island convection in the absence of significant topography. part i: Life cycle of diurnally forced convection. Monthly weather review, 128(10):3459–3480, 2000.

L. Chappel. Assessing severe thunderstorm potential days and storm types in the tropics. In Presentation at the International Workshop on the Dynamics and Forecasting of Tropical Weather Systems, Darwin, 22-26 January 2001, 2001.

T. Dauhut, J.-P. Chaboureau, J. Escobar, and P. Mascart. Giga-LES of hector the convector and its two tallest updrafts up to the stratosphere. Journal of the Atmospheric Sciences, 73(12):5041–5060, 2016.

T. Dauhut, J.-P. Chaboureau, P. Mascart, and T. Lane. The overshoots that hydrate the stratosphere in the tropics. In EGU General Assembly Conference Abstracts, volume 20, page 9149, 2018.

I.-A. Dion, P. Ricaud, P. Haynes, F. Carminati, and T. Dauhut. Ice injected into the tropopause by deep convection–part 1: In the austral convective tropics. Atmospheric Chemistry and Physics, 19(9):6459–6479, 2019.

S. Fueglistaler, A. E. Dessler, T. J. Dunkerton, I. Folkins, Q. Fu, and P. W. Mote. Tropical tropopause layer. Reviews of Geophysics, 47(1), 2009a. doi: 10.1029/2008RG000267. URL https://agupubs.onlinelibrary. wiley.com/doi/abs/10.1029/2008RG000267.

A. J. Geer, F. Baordo,N. Bormann, P. Chambon, S. J. English, M. Kazumori, ... C. Lupu. The growing impact of satellite observations sensitive to humidity, cloud and precipitation. Quarterly Journal of the Royal Meteorological Society, 143(709), 3189-3206, 2017.

R. Goler, M. J. Reeder, R. K. Smith, H. Richter, S. Arnup, T. Keenan, P. May, and J. Hacker. Low-level convergence lines over North Eastern australia. part i: The North Australian cloud line. Monthly weather review, 134(11):3092–3108, 2006.

H. Hatsushika and K. Yamazaki. Interannual variations of temperature and vertical motion at the tropical tropopause associated with ENSO. Geophysical research letters, 28(15):2891–2894, 2001.

H. Hersbach. Operational global reanalysis: progress, future directions and synergies with NWP. European Centre for Medium Range Weather Forecasts, 2018.

R. A. Houze and A. K. Betts. Convection in gate. Reviews of Geophysics, 19(4): 541–576, 1981.

G. J. Huffman, D. T. Bolvin, E. J. Nelkin, D. B. Wolff, R. F. Adler, G. Gu, Y. Hong, K. P. Bowman, and E. F. Stocker. The TRMM multisatellite precipitation analysis (TMPA): quasi-global, multiyear, combined-sensor precipitation estimates at fine scales. Journal of hydrometeorology, 8(1):38–55, 2007.

E. J. Jensen, A. S. Ackerman, J. A. Smith (2007). Can overshooting convection dehydrate the tropical tropopause layer?. Journal of Geophysical Research: Atmospheres, 112(D11), 2007.

C. Liu and E. J. Zipser. Global distribution of convection penetrating the tropical tropopause. Journal of Geophysical Research: Atmospheres, 110(D23), 2005.

C. Liu and E. J. Zipser. Diurnal cycles of precipitation, clouds, and lightning in the tropics from 9 years of TRMM observations. Geophys. Res. Lett., 35, L04819, doi:10.1029/2007GL032437, 2008.

Livesey, N.J., Read,W.G., Wagner, P.A., Froidevaux, L., Lambert, A., Manney, G.L., Millan, L.F., Pumphrey,H.C., Santee, M.L., Schwartz, M.J., Wang, S., Fuller, R.A., Jarnot, R.F., Knosp, B.W.,Martinez, E., and Lay, R.R., Version 4.2x Level 2 data quality and description doc-ument, Tech. Rep. JPL D-33509 Rev. D, Jet Propulsion Laboratory, available at:http://mls.jpl.nasa.gov (last access: 01 09 2019), 2018.

P. Lopez. Direct 4D-Var assimilation of NCEP stage IV radar and gauge precipitation data at ECMWF. Monthly Weather Review, 139(7), 2098-2116, 2011.

B. S. Love, A. J. Matthews, and G. M. S. Lister. The diurnal cycle of precipitation over the maritime continent in a high-resolution atmospheric model. Quarterly Journal of the Royal Meteorological Society, 137(657):934–947, 2011.

L. Millán, W. Read, Y. Kasai, A. Lambert, N. Livesey, J. Mendrok, H. Sagawa, T. Sano, M. Shiotani, and D. L. Wu. Smiles ice cloud products. Journal of Geophysical Research: Atmospheres, 118(12):6468–6477, 2013.

S. Mori, H. Jun-Ichi, Y. I. Tauhid, M. D. Yamanaka, N. Okamoto, F. Murata, N. Sakurai, H. Hashiguchi, and T. Sribimawati. Diurnal land–sea rainfall peak migration over Sumatera island, Indonesian Maritime Continent, observed by TRMM satellite and intensive rawinsonde soundings. Monthly Weather Review, 132(8):2021–2039, 2004.

S. W. Nesbitt and E. J. Zipser. The diurnal cycle of rainfall and convective inten- sity according to three years of trmm measurements. Journal of Climate, 16 (10):1456–1475, 2003.

W. A. Petersen, and S. A. Rutledge. Regional variability in tropical convection: Observations from TRMM. Journal of Climate, 14(17), 3566-3586, 2001.

M. Pope, C. Jakob, and M. J. Reeder. Convective systems of the north australian monsoon. Journal of Climate, 21(19):5091–5112, 2008.

J.-H. Qian. Why precipitation is mostly concentrated over islands in the maritime continent. Journal of the Atmospheric Sciences, 65(4):1428–1441, 2008.

C. S. Ramage. Role of a tropical "maritime continent" in the atmospheric circulation. Mon. Wea. Rev, 96(6):365–370, 1968.

W. J. Randel, F. Wu, H. Voemel, G. E. Nedoluha, and P. Forster. Decreases in stratospheric water vapor after 2001: Links to changes in the tropical tropopause and the brewer-dobson circulation. Journal of Geophysical Re- search: Atmospheres, 111(D12), 2006a.

W.J. Randel and E.J. Jensen. Physical processes in the tropical tropopause layer and their roles in a changing climate. Nature Geoscience, 6:169, 2013. doi: 10.1038/ngeo1733. URL https://doi.org/10.1038/ngeo1733.

S. C. Sherwood. A stratospheric "drain" over the maritime continent. Geophysical research letters, 27(5):677–680, 2000.

A. Stenke and V. Grewe. Simulation of stratospheric water vapor trends: impact on stratospheric ozone chemistry. Atmospheric Chemistry and Physics, 5(5): 1257–1272, 2005.

G. L. Stephens and T. J. Greenwald. The earth's radiation budget and its rela- tion to atmospheric hydrology: 2. observations of cloud effects. Journal of Geophysical Research: Atmospheres, 96(D8):15325–15340, 1991.

G.-Y. Yang and J. Slingo. The diurnal cycle in the tropics. Monthly Weather Review, 129(4):784–801, 2001. 129<0784:TDCITT>2.0.CO;2. doi: 10.1175/1520-0493(2001) URL https://doi.org/10.1175/1520-0493(2001)129<0784:TDCITT>2.0.CO;2.

J. W. Waters, L. Froidevaux, R. S. Harwood, R. F. Jarnot, H. M. Pickett, W. G. Read, ... and J. R. Holden (2006). The earth observing system microwave limb sounder (EOS MLS) on the Aura satellite. IEEE Transactions on Geoscience and Remote Sensing, 44(5), 1075-1092.